


## Optoelectronic Properties of $\text{CuSbS}_2$ and $\text{Cu}_{12}\text{Sb}_4\text{S}_{13}$ Thin Films for Thermoelectric Applications

D. Trejo-Zamudio<sup>a</sup>, M. Morales-Luna<sup>b</sup>, R. Aruna-Devi<sup>a</sup>, C.E. Pérez-García<sup>a</sup> , A. Sosa-Domínguez<sup>a</sup>,  
J.G. Quiñones-Galván<sup>c</sup>, F.J. de Moure-Flores<sup>a</sup>, J. Santos-Cruz<sup>a\*</sup> 

<sup>a</sup>Universidad Autónoma de Querétaro, Facultad de Química, Cerro de las Campanas s/n Col. Las Campanas, 76010, Querétaro, México.

<sup>b</sup>Escuela de Ingeniería y Ciencias, Tecnológico de Monterrey, Av. Eugenio Garza Sada 2501 Sur, Nuevo León, 64849, Monterrey, México

<sup>c</sup>Universidad de Guadalajara, Departamento de Física, Blvd. Marcelino García, 1421, esq Calzada Olímpica, 44430, Guadalajara, México.

Received: November 02, 2022; Revised: February 17, 2023; Accepted: March 30, 2023

This work presents a two-step procedure to obtain thin films with a combination of  $\text{CuSbS}_2$  and  $\text{Cu}_{12}\text{Sb}_4\text{S}_{13}$  phases for study in thermoelectric applications. The procedure consisted of the physical evaporation of sulfides layers ( $\text{Sb}_2\text{S}_3$  and  $\text{CuS}$ ) on glass substrates and the subsequent annealing of the samples in a  $\text{N}_2$  atmosphere. The characterizations by Raman spectroscopy and XRD revealed that the samples presented a varied percentage of  $\text{Cu}_{12}\text{Sb}_4\text{S}_{13}$  and  $\text{CuSbS}_2$ . The results indicated that the percentage of phases depended on the initial thickness of the sulfide layers and the annealing temperature. The lower initial ratio between sulfide thicknesses and annealing temperature above  $300^\circ\text{C}$  favored the formation of  $\text{Cu}_{12}\text{Sb}_4\text{S}_{13}$ . However, the thermoelectric properties were improved when the phases coexisted in the thin film compared to samples with high percentages of  $\text{Cu}_{12}\text{Sb}_4\text{S}_{13}$ . In this way, a sample with a power factor of  $2.30 \mu\text{W}/\text{cm}\cdot\text{K}^2$  at  $60^\circ\text{C}$  was identified.

**Keywords:**  $\text{CuSbS}_2$  chalcostebite,  $\text{Cu}_{12}\text{Sb}_4\text{S}_{13}$  tetrahedrite, thin films, thermoelectric.

### 1. Introduction

Thermoelectric materials are those that can take advantage of the Seebeck, Peltier and Thompson effects to convert heat into electrical energy or take advantage of a current passing through them to heat or cool. These materials are small, reliable, environmentally friendly; also, they do not produce noise or vibrations, can operate in wide temperature range, and have a long period of life<sup>1-3</sup>. However, for a material to be a good thermoelectric, it must have a good efficiency, which is determined by the figure of merit  $ZT$ , which is given by the equation:

$$ZT = S^2\sigma T / K \quad (1)$$

where  $S$  is the Seebeck coefficient, sometimes denoted by  $\alpha$ ,  $\sigma$  is the electrical conductivity and  $K$  is the thermal conductivity and  $T$  is the working temperature<sup>2</sup>. The higher the  $ZT$  value, the more efficient the material. To improve the  $ZT$  value, the thermal conductivity can be reduced with the help of nanoprecipitates, nano-inclusions to disperse the phonons or with material of complex structure that reduce the mean free path of the phonon. The other option is the improve of the power factor (PF),  $S^2\sigma$ . The PF value has been improved through the regulation the convergence of electronic band structure, resonance levels and invisible dopants<sup>3</sup>.

Currently, the materials that have been studied for thermoelectric applications are varied, and most of them, are based on compounds derived from lead, selenium, or tellurium. However, some of these materials can be toxic and dangerous for the environment, especially those based on lead, so new alternatives to these materials have been studied. Alternatives include bismuth, copper, and sulfur compounds. Recent investigations have even focused on the study of essential aspects, and little studied, such as the effects of corrosion, the mechanical characteristics and the electrochemical responses in compounds based on bismuth telluride, given the good thermoelectric properties of this material<sup>4-6</sup>. However, some copper and sulfur compounds, as well as ternary compounds with antimony and selenium, have been little studied and have potential use in photovoltaic and thermoelectric applications. In the case of ternary compounds of Cu-Sb-S,  $\text{CuSbS}_2$  has been studied for thermoelectric applications<sup>7</sup>.  $\text{CuSbS}_2$  (chalcostebite) is a material with advantages, the elements that compose it are abundant on the earth, they are low-toxic and they are economics<sup>8</sup>.  $\text{CuSbS}_2$  compound is a  $p$ -type semiconductor, with a direct optical band gap of 1.4 to 1.6 eV, with a hole density of  $10^{15}$  to  $10^{18} \text{cm}^{-3}$ <sup>8-11</sup>. Although there are various procedures to obtain thin films by thermal evaporation, either by individual elements<sup>12</sup>, few investigations have focused on obtaining thin films through the sequential evaporation of two sulfides<sup>8,13</sup>.

\*e-mail: [jsantos@uaq.edu.mx](mailto:jsantos@uaq.edu.mx)

However, the most studied applications are for photoelectric purposes and as a thermoelectric material, there are not many reports, being the solid-state reaction technique used to obtain pellets and be studied at high pressure to know their optical properties and structural; as well as determine a possible use in thermoelectric devices<sup>7</sup>. Although the main challenge in the preparation of CuSbS<sub>2</sub> films is the presence of secondary phases such as Sb<sub>2</sub>S<sub>3</sub> (stibnite), CuS (covellite), Cu<sub>18</sub>S (digenite), Cu<sub>3</sub>SbS<sub>3</sub> (skinnerite), Cu<sub>3</sub>SbS<sub>4</sub> (famatinitite) and Cu<sub>12</sub>Sb<sub>4</sub>S<sub>13</sub> (tetrahedrite), which are present regardless of the process or technique used<sup>8,12,14,15</sup>. Of these, it is tetrahedrite (Cu<sub>12</sub>Sb<sub>4</sub>S<sub>13</sub>), which is also interesting to be used as a thermoelectric. In other works, the tetrahedrite has easily formed in a Cu-rich environment<sup>10,16,17</sup>. This phase has been obtained in thin film by the electron beam evaporation technique, with a reported *p*-type conductivity, a direct optical band gap of 1.8 eV and a power factor greater than 1.0, as well as a charge carrier concentration of up to ( $\sim 10^{20} \text{ cm}^{-3}$ )<sup>17</sup>. In some cases, Seebeck coefficient values of 80  $\mu\text{V/K}$  or more have been reported for a temperature of 300 K in powders and 56.69  $\mu\text{V/K}$  to 340 K in thin films, with PF values of 2.30  $\mu\text{W/cm}\cdot\text{K}^2$  at 495 K<sup>3,17</sup>. The obtaining of CuSbS<sub>2</sub> and Cu<sub>12</sub>Sb<sub>4</sub>S<sub>13</sub> as thin films by the Physical Vapor Deposition (PVD) technique is of interest in this work. This kind of deposit has been used to obtain these phases by means of sequential evaporation of sulfides and using a subsequent annealing. Also, it has been reported that both phases can be found when the concentration of CuS is varied<sup>8,16</sup>.

This work describes the process to obtaining thin films of CuSbS<sub>2</sub> and Cu<sub>12</sub>Sb<sub>4</sub>S<sub>13</sub> for thermoelectric applications; this through a process similar described by Medina-Montes et. al. and Trejo-Zamudio et. al. The process consisted of a sequential evaporation of antimony and copper sulfides on glass substrates. The proportion of copper sulfide was varied accordingly with stoichiometry of the compound and the annealing temperature. The samples obtained were characterized by Raman spectroscopy, Ultraviolet-Visible Spectroscopy, EDS, Hall effect, X-ray Diffraction, Scanning Electron Microscope and X-Ray Photoelectron Spectrometry. Thin films of combined phases with a high Seebeck coefficient and power factor, for use as *p*-type material in thermoelectric modules, were obtained.

## 2. Experimental Details

### 2.1. Preparation of Cu-Sb-S films

Ternary chalcogenide films were obtained by a procedure similar to that described by Medina-Montes et al.<sup>8</sup> and Trejo-Zamudio et al.<sup>16</sup>. The procedure consisted of two main stages: the sequential deposit of sulfide films and the thermally annealed of the films in a N<sub>2</sub> atmosphere.

Glass substrates of 7.5 cm x 2.5 cm were cleaned with soap, rinsed with distilled water several times, and treated with a chromic solution acid for 24 hours. Subsequently, the substrates were rinsed with deionized water and treated with a 3:1 mixture of water and nitric acid for additional 3 hours close to the boiling point solution. The substrates were rinsed with deionized water several times and stored in an amber glass recipient with deionized water and ethanol.

In the first stage, by means of the physical evaporation deposit technique, a layer of antimony (III) sulfide (Sb<sub>2</sub>S<sub>3</sub>) followed by a layer of cooper (II) sulfide (CuS) were deposited in a sandwich structure on the glass substrate. Pure Sigma-Aldrich powders were used in this work. The growth of the films was at room temperature. The vacuum pressure to start the deposit was  $6 \times 10^{-5}$  mbar and the distance between the source to the substrate was kept constant at 16 cm. The applied current for the antimony and copper sulfide was 120 and 210 A respectively. The deposit was in two stages, first the antimony sulfide, the vacuum is removed, and the copper sulfide is placed and deposited under the same conditions described. Finally, the sample obtained has a structure: glass substrate/Sb<sub>2</sub>S<sub>3</sub>/CuS.

The thicknesses of the Sb<sub>2</sub>S<sub>3</sub> were adjusted at 320 nm and CuS film was varied by approximately 160, 180, 200 and 220 nm. The thickness ratio between the Sb<sub>2</sub>S<sub>3</sub> and CuS were 2.00, 1.78, 1.60 and 1.45. Each sample was labeled as CuSbS 2.00, CuSbS 1.78, CuSbS 1.60 and CuSbS 1.45. The thicknesses of the samples were measured by profilometry. The second stage consisted of a thermal annealing at 250, 300, 350 and 400 °C in a quartz tubular furnace of Lindberg Blue M. An atmosphere of N<sub>2</sub> gas was employed for 2 h. Table 1 summarizes the conditions in which the samples were obtained and the name of the samples.

### 2.2. Characterization techniques

The Cu-Sb-S chalcogenide samples were characterized for study as thermoelectric material. The thicknesses of the samples were measured with an Alpha-Step D-100 KLA Tencor. Raman spectra were acquired with a Thermo Scientific DXR2 system equipped with a 633 nm laser as excitation source. X-ray diffractograms, to determine the structure of the materials, were obtained with an Empyrean diffractometer using a Cu K $\alpha$  radiation ( $\lambda=1.5406 \text{ \AA}$ ). The transmittance of films was measured using Genesys 10 S UV-VIS, Thermo Scientific. The electric properties were measured using a Hall Effect Measurement System (ECOPIA HMS-300). Elemental composition of the samples was determined by energy dispersive spectroscopy, EDS analysis, in a Hitachi SU1510. The chemical states of the elements present in the material deposited were analyzed by XPS, in a XPS Escalab 250 Xi (ThermoFisher). The Seebeck coefficient of the samples

**Table 1.** Conditions of deposit CuSbS samples.

Sample	Film thickness (nm)		Annealing temperature °C/ (2 h)
	Sb <sub>2</sub> S <sub>3</sub>	CuS	
CuSbS 1.45/250	320	220	250
CuSbS 1.45/350	320	220	350
CuSbS 1.45/400	320	220	400
CuSbS 1.60/350	320	200	350
CuSbS 1.60/400	320	200	400
CuSbS 1.78/300	320	180	300
CuSbS 1.78/350	320	180	350
CuSbS 2.00/250	320	160	250
CuSbS 2.00/300	320	160	300
CuSbS 2.00/350	320	160	350
CuSbS 2.00/400	320	160	400

was measured using a system made up of Peltier devices and a Keithley 740 microvoltmeter. Finally, the surface morphology was acquired by scanning electron microscopy using a field scanning electron microscope (SEM) Model Nova NanoSEM 200, FEI. The power factor was obtained by multiplying the electrical conductivity of the sample by square of the Seebeck coefficient ( $S^2\sigma$ ).

### 3. Results and Discussion

#### 3.1. Raman characterization

Figure 1 (a-d) shows the Raman spectra of the samples, where two signals are observed that correspond to vibrational modes with centers marked at 335 and 356  $\text{cm}^{-1}$ , attributable to  $\text{CuSbS}_2$  and  $\text{Cu}_{12}\text{Sb}_4\text{S}_{13}$  compounds respectively<sup>7,8,16,18,19</sup>. The signal at 335  $\text{cm}^{-1}$  is attributable to stretching vibrational mode from the Sb-S bond in  $\text{CuSbS}_2$  and is close to that reported at 329  $\text{cm}^{-1}$ <sup>18</sup>. The Raman band at 356  $\text{cm}^{-1}$  has been reported in the literature<sup>8,19</sup> and might be related with the stretching vibrations of Sb-S bond in tetrahedrite structure<sup>8,19,20</sup>. The Raman spectra show that the two phases,  $\text{CuSbS}_2$  and  $\text{Cu}_{12}\text{Sb}_4\text{S}_{13}$ , coexist in the samples, in some with a higher proportion than the others and depends on the temperature and the initial sulfide ratio. The samples  $\text{CuSbS}$  2.00 at 350 °C and  $\text{CuSbS}$  2.00 at 400 °C samples present the  $\text{CuSbS}_2$  phase in greater quantity than the other samples. Not so with the samples  $\text{CuSbS}$  2.00 at 250 °C and 300 °C, which have the  $\text{CuSbS}_2$  phase to a lesser extent. Therefore, it can be predicted that a greater amount of initial CuS, a greater amount of Cu, favors the formation of tetrahedrite phase, when the annealing temperatures exceed 350 °C. This confirms previous studies where it has been reported that an excess of CuS (excess of Cu) with respect to  $\text{Sb}_2\text{S}_3$  favors the formation of  $\text{Cu}_{12}\text{Sb}_4\text{S}_{13}$ <sup>8,12,15,16</sup>. The other

samples present only a signal related with the  $\text{Cu}_{12}\text{Sb}_4\text{S}_{13}$  at 356  $\text{cm}^{-1}$ , although a low intensity signal can be seen at 335  $\text{cm}^{-1}$ , which corresponds to chalcocite. Some samples show a shift to the right, such as  $\text{CuSbS}$  1.45 at 250 °C,  $\text{CuSbS}$  2.00 at 300 °C and  $\text{CuSbS}$  1.45 at 350 °C. This could indicate stress in the lattice of material since no other signals are observed that indicate the presence of secondary phases. The full width at half maximum (FWHM) of the signal also indicates that the crystalline quality of the material is lower with respect to other samples. In the sample  $\text{CuSbS}$  1.78 at 300 °C and 350 °C, a band with center at 326  $\text{cm}^{-1}$  is observed, which may be due to the presence of  $\text{Cu}_3\text{SbS}_4$ , and it has even reported that a vibrational mode at 330  $\text{cm}^{-1}$  may be due to presence of  $\text{Cu}_3\text{SbS}_4$ <sup>15,17</sup>; although it could also be due to stoichiometry deficiency or presence of the  $\text{CuSbS}_2$  phase. No bands corresponding to secondary binary phases were found, such as CuS at 470  $\text{cm}^{-1}$  as explained Medina-Montes et. al, which might indicate that there are no remains of the precursors in the samples<sup>8,21</sup>.

According to Medina-Montes and collaborators, the Raman data in Figure 1 can be used to quantify the percentage of phases contained in the sample, for this is necessary to exclude the part of  $\text{Sb}_2\text{S}_3$  that did not react. Based on this, the following equation was employed:

$$Area_{Cu-Sb-S}(\%) = \frac{Area_{Cu-Sb-S}}{Area_{CuSbS_2} + Area_{Cu_{12}Sb_4S_{13}}} \times 100 \quad (2)$$

Where  $Area_{Cu-Sb-S}$  is the area of Raman band at either 335  $\text{cm}^{-1}$  ( $Area_{CuSbS_2}$ ) or 356  $\text{cm}^{-1}$  ( $Area_{Cu_{12}Sb_4S_{13}}$ )<sup>8</sup>.

Figure 2 shows the results of the percentage of estimated phases found in each sample. It was necessary to deconvolve the signals at 335 and 356  $\text{cm}^{-1}$ .

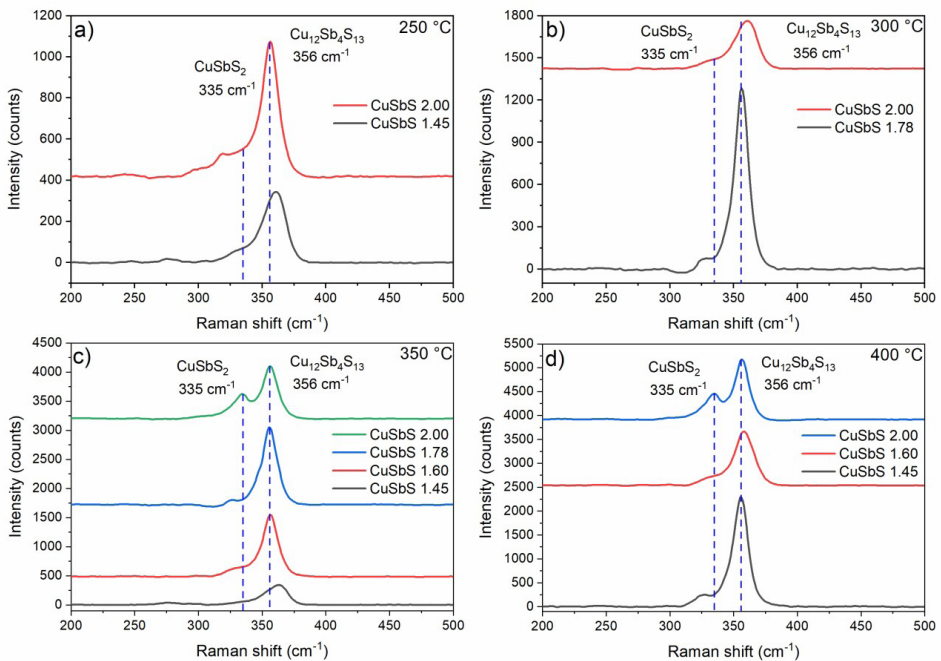


**Figure 1.** Raman spectra of  $\text{CuSbS}$  samples a) 250 °C, b) 300 °C, c) 350 °C and d) 400 °C.

According to the results, it can be observed that when the CuS ratio increase, there is a greater amount of Cu, which favors the formation of  $\text{Cu}_{12}\text{Sb}_4\text{S}_{13}$ . This can be seen in Figure 2a, 2b, and 2d. Where it is observed that the percentage of  $\text{Cu}_{12}\text{Sb}_4\text{S}_{13}$  increases and the percentage of  $\text{CuSbS}_2$  decreases when the initial concentration of Cu increases, and the annealing temperature is constant. However, the percentages are very similar to those obtained in another investigation, where at 250 °C and a sulfide ratio of 2.5, close to 20% of  $\text{CuSbS}_2$  was obtained<sup>8</sup>.

Figure 2c shows that by increasing the amount of CuS, the percentage of  $\text{Cu}_{12}\text{Sb}_4\text{S}_{13}$  obtained increase with respect to the other temperatures, such as the sample CuSbS 1.45 annealed at 250, 350 and 400 °C, as well as in the samples CuSbS 1.78 annealed at 300 and 350 °C and for the CuSbS 1.60 samples the results are similar. However, with the sample CuSbS 2.00, the opposite occurs when the temperature increase. This could be due to the fact that a percentage of  $\text{Cu}_{12}\text{Sb}_4\text{S}_{13}$ , that has been formed, reacts with  $\text{Sb}_2\text{S}_3$  to form  $\text{CuSbS}_2$ <sup>8</sup>. This is likely since the samples contain a higher proportion of  $\text{Sb}_2\text{S}_3$  than the other samples. Furthermore, in Figure 2c, it is observed that the maximum percentage of  $\text{Cu}_{12}\text{Sb}_4\text{S}_{13}$  obtained was 97% very close to the 96% obtained with the same initial sulfide ratio at 300 °C. However, as the proportion of sulfurs decreases (CuS increases), the percentage of  $\text{CuSbS}_2$  increases again, maybe part of the tetrahedrite could be decompose into  $\text{CuSbS}_2$  and  $\text{Sb}_2\text{S}_3$ . Although the latter could be in smaller quantity and a signal in Raman is no appreciated, in addition, only the areas of two signals were used in the calculations.

### 3.2. XRD characterization

Figure 3 (a-d) shows the XRD patterns of the annealed samples. The XRD patterns of the samples were compared with

the corresponding cards, PDF#44-1417 and PDF#24-1318 for  $\text{CuSbS}_2$  (orthorhombic) and  $\text{Cu}_{12}\text{Sb}_4\text{S}_{13}$  (cubic) respectively. These phases were the only detected by XRD and Raman.

Figure 3a) shows that as the initial thickness of copper sulfide film increases, the tetrahedrite phase is favored if the annealing is carried out at the same temperature. The same is observed in the other diffractograms, Figure 3b and Figure 3d, where the samples with a lower ratio between thickness are those in which the  $\text{Cu}_{12}\text{Sb}_4\text{S}_{13}$  phase is favored. The samples CuSbS 1.78 at 300 and 350 °C show the tetrahedrite phase and the (111) plane in not displayed. The CuSbS 2.00 samples present both phases coexist at different temperatures, which coincides with Medina-Montes and collaborators<sup>8</sup>.

The other samples show the presence of both phases coexisting as CuSbS 1.60 and CuSbS 1.45. It is also observed that there is a slight shift to the right of the diffraction patterns of the samples with respect to the cards, indicating stress within the samples. The samples showing the tetrahedrite phase match with the planes (200) at  $2\theta = 17.170^\circ$ , (220) at  $2\theta \approx 24.366^\circ$ , (222) at  $2\theta \approx 29.950^\circ$ , (321) at  $2\theta \approx 32.411^\circ$ , (400) at  $2\theta \approx 34.714^\circ$ , (330) at  $2\theta \approx 36.899^\circ$ , (440) at  $2\theta \approx 49.902^\circ$  and (622) at  $2\theta \approx 59.303^\circ$  of the PDF cards. In the samples in which the two phases are observed, some of the planes listed above can be observed, however, the signals corresponding to the planes (200) at  $2\theta \approx 12.102^\circ$ , (111) at  $2\theta \approx 28.447^\circ$ , (410) at  $2\theta \approx 28.728^\circ$ , (301) at  $2\theta \approx 29.909^\circ$  and (212) at  $2\theta \approx 52.033^\circ$  are also appreciated with less intensity. These last planes belong to the  $\text{CuSbS}_2$  phase of the card PDF#44-1417.

In general, the XRD results coincide with those obtained in Raman spectroscopy, since it is shown that by increasing the amount of CuS (greater amount of Cu), the formation of tetrahedrite is favored. Likewise, the CuSbS 1.78 samples annealed at 300 and 350 °C are those that presented the highest percentage of tetrahedrite.

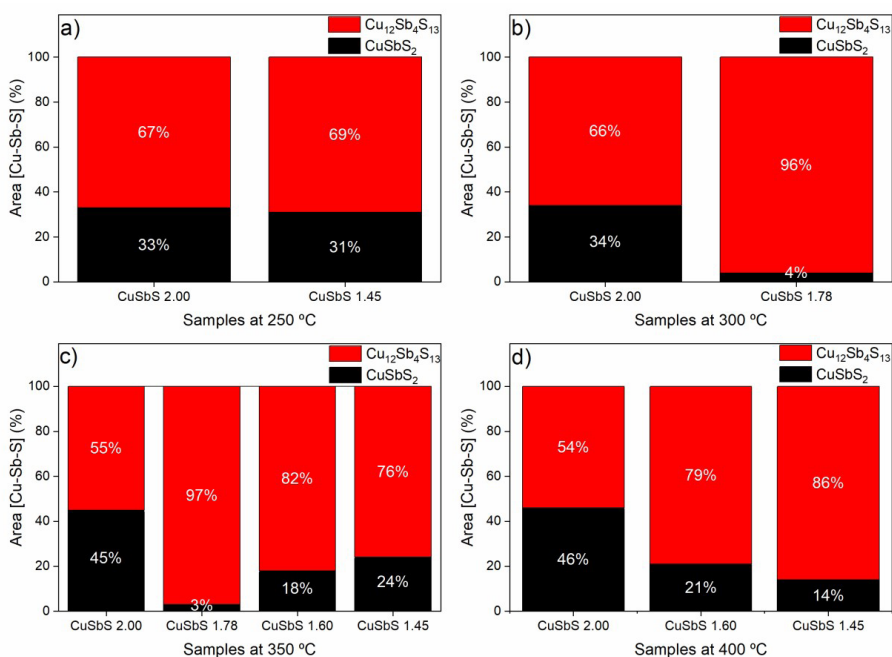


**Figure 2.** Phases content in the CuSbS samples a) 250 °C, b) 300 °C, c) 350 °C and d) 400 °C.

With the diffractograms of Figure 3, the average size of the crystals ( $D$ ) was calculated. For this, the Debye-Scherrer equation was employed:

$$D = \frac{0.9\lambda}{\beta \cos\theta} \quad (3)$$

Where  $D$  is the average of the crystallite size,  $\lambda = 1.5406 \text{ \AA}$  is the Cu  $K_\alpha$  radiation,  $\theta$  is Bragg angle and  $\beta$  is the full-width at half maximum of diffraction peak<sup>22</sup>. The results are presented in the Table 2. The results are very similar

with respect to other studies, in this case the crystallite size is smaller compared to the study by Medina-Montes et. al. This difference could be due to difference in the thickness of  $\text{Sb}_2\text{S}_3$  used. In this study the thickness used was 320 nm, less than 400 nm, used in the other study. This could cause the films to have a lower crystallization quality and cause a small crystallite size, because they have less material and could evaporate in the annealing process, affecting the crystalline quality of the samples. Also, having less material, the crystal does not grow as when a greater amount of  $\text{Sb}_2\text{S}_3$  is available.

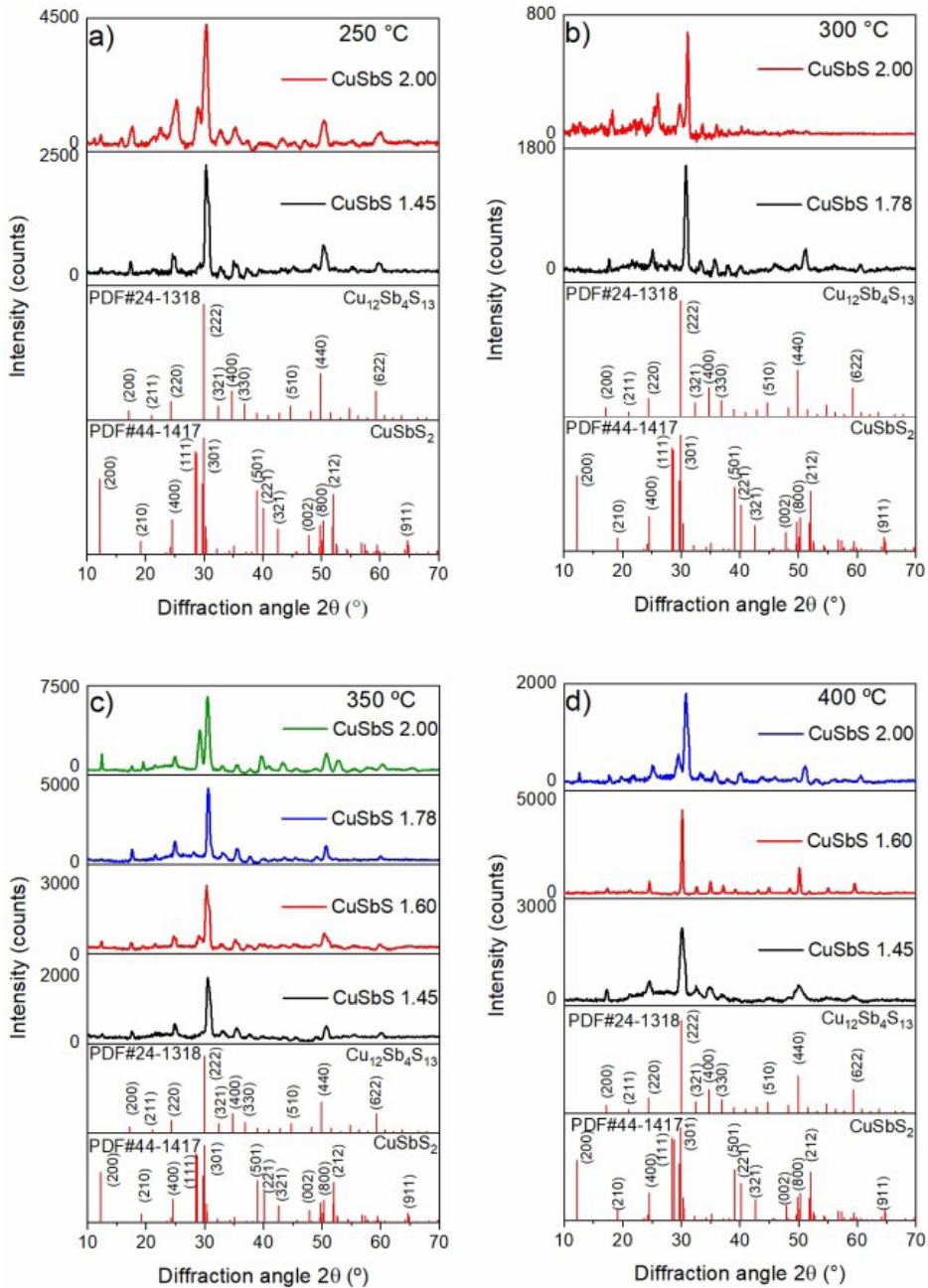


**Figure 3.** XRD patterns of the  $\text{CuSbS}$  samples after of the annealing at a) 250 °C, b) 300 °C, c) 350 °C and d) 400 °C.

**Table 2.** Elemental composition, crystallite size and thickness of CuSbS samples.

Sample/Annealing temperature	(% Atomic + SD)			Crystallite size (nm)	Thickness of samples (nm)
	Cu	Sb	S		
CuSbS 2.00/250	54.62 + 0.30	11.17 + 0.32	34.21 + 0.01	21	430
CuSbS 1.45/250	53.13 + 0.16	11.01 + 0.32	35.86 + 0.16	22	480
CuSbS 2.00/300	55.81 + 1.66	11.10 + 0.41	33.09 + 1.26	28	420
CuSbS 1.78/300	59.36 + 0.25	8.23 + 0.29	32.42 + 0.04	25	430
CuSbS 2.00/350	49.55 + 0.46	13.90 + 0.92	36.55 + 0.46	22	400
CuSbS 1.78/350	58.99 + 0.69	8.46 + 0.19	32.55 + 0.49	28	410
CuSbS 1.60/350	52.15 + 1.05	11.49 + 0.84	36.36 + 0.21	29	440
CuSbS 1.45/350	54.09 + 0.17	10.85 + 0.16	35.06 + 0.33	18	450
CuSbS 2.00/400	47.93 + 0.42	13.88 + 0.01	38.19 + 0.44	18	400
CuSbS 1.60/400	54.00 + 0.28	11.84 + 0.71	34.16 + 0.42	26	430
CuSbS 1.45/400	55.87 + 0.81	9.44 + 0.23	34.69 + 0.58	18	440
<b>Cu<sub>12</sub>Sb<sub>4</sub>S<sub>13</sub>*</b>	<b>41.38</b>	<b>13.79</b>	<b>44.83</b>		
<b>CuSbS<sub>2</sub>*</b>	<b>25.00</b>	<b>25.00</b>	<b>50.00</b>		

\*Ideal composition.

### 3.3. EDS Analysis

Table 2 shows the elemental composition of the samples determined by EDS. All samples were measured at two different points to determine their homogeneity. Figure 4 shows the EDS analysis for some samples, the figure includes the two measurements in different regions of the thin film. The results shown in Table 2 represent the average of the two measurements and the standard deviation (SD). The SD has small values, which indicates homogeneous distribution of the material in the thin films obtained.

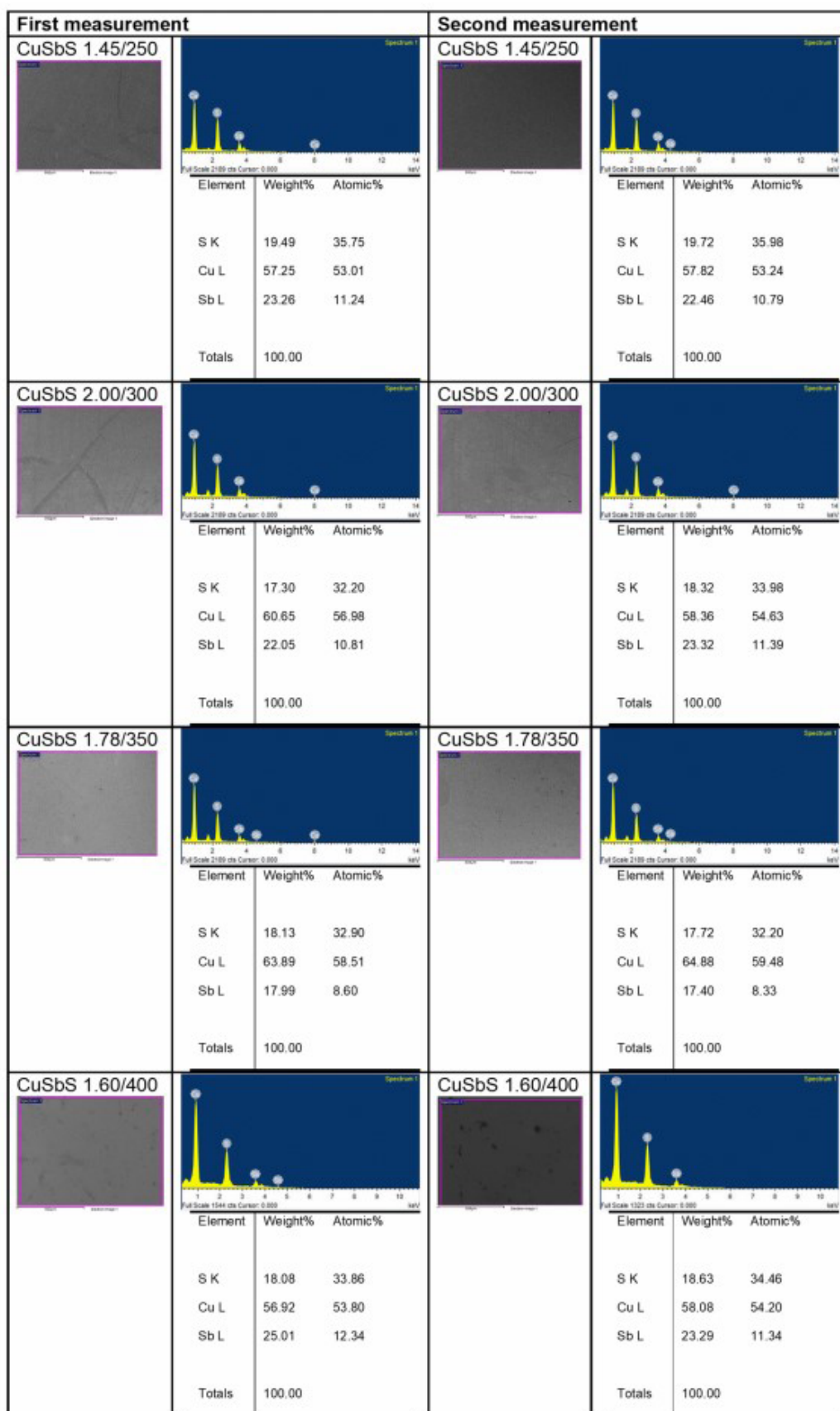
As can be seen, all the samples show an excess of Cu with respect to the ideal composition of chalcocite and tetrahedrite. Remembering that the samples that present a high percentage of Cu<sub>12</sub>Sb<sub>4</sub>S<sub>13</sub> are the CuSbS 1.78 samples that were annealed at 300 and 350 °C, these samples present more than a 10% excess of Cu with respect to the ideal stoichiometry. This can affect the electrical properties of the material. Tetrahedrite is a *p*-type semiconductor and holes are provided by sulfur atoms, by reducing its percentage, the electrical conductivity is affected, since it has a lower charge carrier concentration with respect to the ideal stoichiometry<sup>3,16</sup>.

In these same samples antimony does not have many changes, but sulfur has deficiencies, this due to the annealing process, by which sulfur evaporates first, followed by antimony and copper. The other samples show an excess of Cu as well, which is explained by the annealing process and the evaporation of sulfur. It should also be considered that the samples show both phases coexisting. In the case of the CuSbS 2.00 samples annealed at 350 and 400 °C, they are those that have an atomic percentage close to ideal but are the samples that present the highest percentage of chalcocite. In a balance of the two phases, the amount of Cu is lower and therefore close to the ideal, but, both phases present an excess of Cu. One likely way to find an ideal stoichiometry sample using this method would be to reduce anneal times to avoid sulfur loss. As well as an annealing

using high pressure with an inert gas to avoid the loss of antimony and sulfur or in a closed system. Also, annealing could be carried out in a sulfur atmosphere.

### 3.4. Optical absorption

Figure 5 shows the spectral transmittance curves of the CuSbS samples prepared with different Sb<sub>2</sub>S<sub>3</sub>/CuS ratios and annealed at different temperatures. The CuSbS 1.78/350 sample presents the highest transmittance in the region from 800 to 1000 nm and the CuSbS 2.00/400 sample presents the lowest transmittance. The first sample only presents the 3% of CuSb<sub>2</sub> and the second the 54% of CuSbS<sub>2</sub>. According with the literature the fundamental absorption edge of CuSbS<sub>2</sub> is at ~ 900 nm<sup>23,24</sup>, although it could be exhibited since the 750 nm. For the Cu<sub>12</sub>Sb<sub>4</sub>S<sub>13</sub> is at ~ 600 nm<sup>17</sup>. The samples CuSbS 2.00 and 1.45 annealed at 250 °C show a similar transmittance curve, with an absorption edge close at 600-650 nm and another close at 700 nm. These samples contain a similar percentage of CuSbS<sub>2</sub> but in Raman spectroscopy the second showed a shift to the right, so the crystalline quality of the sample could be lower or could indicate stress in the crystal lattice or could be another phase (although in XRD no other was found). This difference can cause the edge to shift to the right and show higher transmittance with respect to the CuSbS 2.00 sample, the higher wave in its spectrum, could confirm a good crystallinity and homogeneous grain growth of the films<sup>15</sup>. Therefore, the effect observed in Raman may be due to stress in the lattice. The samples annealed at 300 °C have a different transmittance curve. The CuSbS 1.78 sample shows an absorption edge at ~ 550-600 nm which could be attributable to the presence of tetrahedrite and an interference wave close at 700 nm attributable to the thickness<sup>25</sup>. On the other hand, the CuSbS 2.00 sample presents absorption edge after 600 nm and another close at 650 nm, since it contains a 45% of chalcocite. This last sample has a transmittance spectrum like samples annealed at 250 °C that contain around

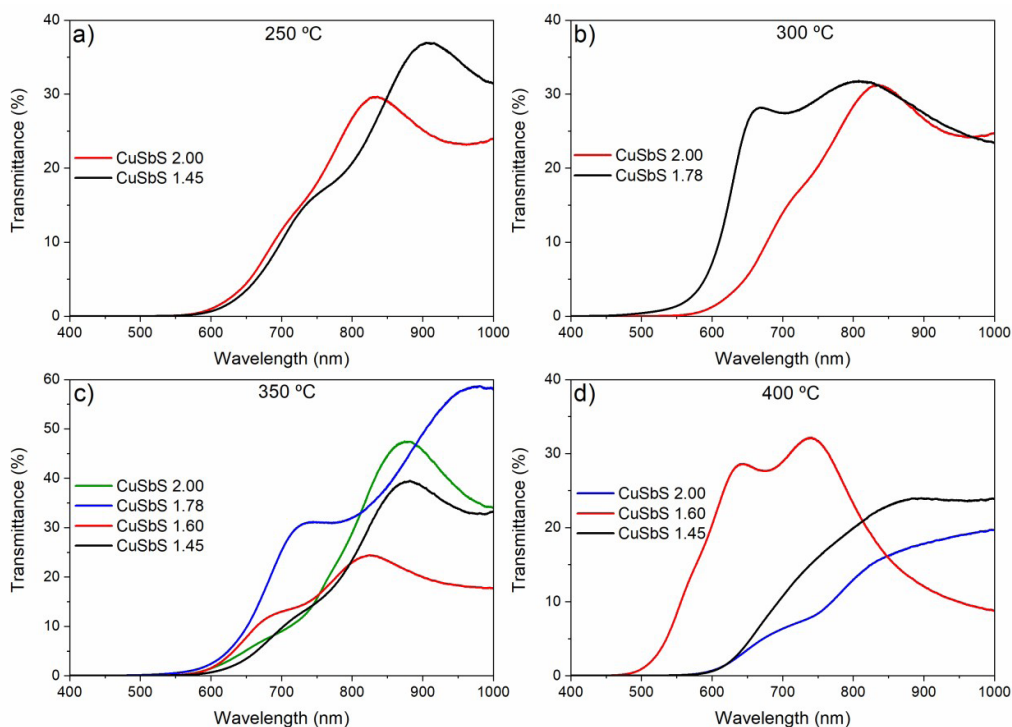

 Figure 4. EDS analysis of the  $\text{CuSbS}$  1.45/250,  $\text{CuSbS}$  2.00/300,  $\text{CuSbS}$  1.78/350 and  $\text{CuSbS}$  1.60/400 samples.

30% of the secondary phase ( $\text{CuSb}_2$ ). The  $\text{CuSbS}$  1.78 sample annealed at  $350^\circ\text{C}$  has a similar transmittance spectrum as the  $\text{CuSbS}$  1.78 sample annealed at  $300^\circ\text{C}$ . This sample also contains a low percentage of the secondary phase (4%) and has a lower thickness which represents a higher percentage of transmittance. Also, the second sample has a larger crystal size and higher wave in its spectrum, confirming a good crystallinity and homogeneous grain growth of the films<sup>15</sup>. The  $\text{CuSbS}$  2.00, 1.60 and 1.45 samples annealed at  $350^\circ\text{C}$  have an absorption edge close at 600 nm and to a lesser intensity at  $\sim 650$ -750 nm, since these contain chalcocite in a higher percentage. The samples  $\text{CuSbS}$  2.00 and 1.45 are very similar because the percentage of chalcocite phase in these sample is higher than the  $\text{CuSbS}$  1.60 sample. Also, the wave is higher in the curve of the  $\text{CuSbS}$  2.00 sample because it has a larger crystal size.

Finally, the Figure 5d shows the transmittance spectra of the samples annealed at  $400^\circ\text{C}$ . The sample  $\text{CuSbS}$  1.60 has a spectrum very similar to that of the samples  $\text{CuSbS}$  1.78/300 and  $\text{CuSbS}$  1.78/350, although the absorption edge is close to 500 nm. This sample has 21% of  $\text{CuSbS}_2$ , according to results in Raman spectroscopy, but in XRD analysis it showed tetrahedrite as the main phase and a larger crystal size, which explain a higher transmittance with respect to the rest of the samples annealed at  $400^\circ\text{C}$ . The spectra of the  $\text{CuSbS}$  2.00 and 1.45 samples are similar, both contain chalcocite in a percentage greater than 10%. It is the reason why these samples present an absorption edge above 600 nm. The  $\text{CuSbS}$  2.00 sample has a lower intensity edge near at 700 nm, which confirm the presence of chalcocite. Its spectrum is like that of other samples with

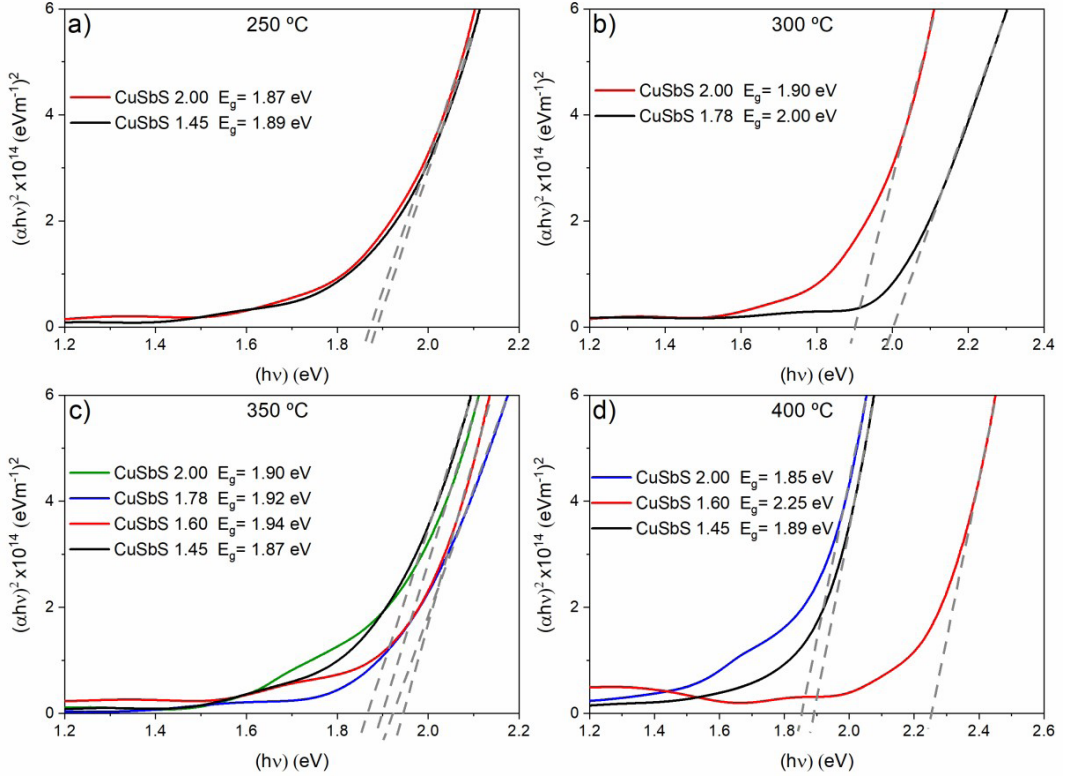
the same  $\text{CuS}/\text{Sb}_2\text{S}_3$  ratio and annealed at other temperature but with lower transmittance. This may be because it has a smaller crystal size and may be a less homogenous sample in the growth of its grains.

Figure 6 displays the direct optical band gap for the  $\text{CuSbS}$  samples. For this, the Beer-Lambert law was used to calculate the absorbance and the absorption coefficient  $\alpha$ . Subsequently, the band gap was estimated using the Tauc parabolic bands model. Figure 6 shows the extrapolation of the linear region of  $(\alpha h\nu)^2$  versus  $h\nu$  to the x-axis. According with Figure 6, the band gap of the  $\text{CuSbS}$  samples is in the range of 1.85 to 2.25 eV; values very close to those reported in the literature<sup>17,19,26</sup>. According to reports the band gap of  $\text{Cu}_{12}\text{Sb}_4\text{S}_{13}$  can be influenced by many factors<sup>17</sup>. The band gap can vary due to the effect of decreasing particle size and it can increase<sup>26</sup>. In other cases, it has been reported that the band gap increases when the samples are rich in Cu, in these cases the highest value reported has been of 1.9 eV<sup>27</sup>. Prem Kumar et. al. reported values of 1.84 eV for samples with mixes of phases ( $\text{Cu}_{12}\text{Sb}_4\text{S}_{13}$  and  $\text{Cu}_3\text{SbS}_4$ ) and rich in Cu ( $\sim 55\%$  Cu and  $\sim 37\%$  S) and a value of 1.93 eV for a sample rich in S ( $\sim 42\%$  S)<sup>17</sup>. In this work, the samples that contain the highest percentage of tetrahedrite are the  $\text{CuSbS}$  1.78/300 and  $\text{CuSbS}$  1.78/350, and these samples are rich in Cu ( $\sim 59\%$ ) and present values of band gap of 2.00 eV and 1.92 eV respectively. These values agree with the reported for similar samples. Also, the sample with the lowest band gap is  $\text{CuSbS}$  2.00/400, but this sample is rich in S with respect to the other samples. However, it is a sample that contain a high percentage of  $\text{CuSbS}_2$  and as the band gap of this phase is smaller, that is why the band gap of the sample



**Figure 5.** Transmittance spectra of  $\text{CuSbS}$  samples annealed at a)  $250^\circ\text{C}$ , b)  $300^\circ\text{C}$ , c)  $350^\circ\text{C}$  and d)  $400^\circ\text{C}$ .





**Figure 6.** Tauc plots of CuSbS films,  $(\alpha hv)^2$  versus  $hv$  energy.

decreases. The values are similar for the other samples with the same initial ratio of CuS/Sb<sub>2</sub>S<sub>3</sub>. The sample with the highest band gap is CuSbS 1.60/400, its value is 2.25 eV. This sample contains 79% of tetrahedrite, is rich in Cu and has a small crystal size, this in combination could explain the increased of band gap. This in contrast to the samples that have the same initial sulfides ratio (CuSbS 1.45/350 and CuSbS 1.45/250); these samples have a smaller band gap but contain a higher percentage of chalcocite. Finally, the samples CuSbS 1.60/350 and CuSbS 1.45/400 have band gap values of 1.94 eV and 1.89 eV respectively, are similar values. The samples have similar percentage of Cu<sub>12</sub>Sb<sub>4</sub>S<sub>13</sub>, Cu and S. However, the CuSbS 1.60/350 sample have a larger crystal size; this could explain the higher value of band gap.

### 3.5. Electrical characterization

Table 3 shows the results of the electrical measurements carried out using the Hall effect. Samples of 1x1 cm were employed in the van der Pauw configuration and the thickness of the samples used in the characterization are showed in Table 2. According to the results shown in the table, it can be confirmed that the samples present the two phases coexisting. This is because the charge carrier concentration is greater than the CuSbS<sub>2</sub> phase and less than the Cu<sub>12</sub>Sb<sub>4</sub>S<sub>13</sub> phase. The charge carrier concentration reported for CuSbS<sub>2</sub> is  $10^{15}$  to  $10^{18} \text{ cm}^{-3}$ <sup>8-11</sup> and for Cu<sub>12</sub>Sb<sub>4</sub>S<sub>13</sub> is up to  $10^{20} \text{ cm}^{-3}$ . When there is a secondary phase, this affects the charge carrier concentration of the main phase<sup>28</sup>. In this case, this parameter is affected by the percentage of the phases and by

the amount of Cu and S. In some samples the charge carrier concentration drops to  $10^{20} \text{ cm}^{-3}$  (CuSbS 1.78/350, 1.45/250, 1.45/350, 1.45/400) which are samples that contain high amounts of Cu and low amounts of S; all three samples also have a crystal size less than 20 nm. It agrees with another study where it is explained that theoretically decreasing sulfur element decrease the charge carrier concentration<sup>3</sup>. These same samples have a lower conductivity with respect to the others. The CuSbS 2.00/300 sample, also has lower charge carrier concentration but also has a high concentration of Cu, this effect is not observed in the CuSbS 2.00/250, CuSbS 1.78/300 and CuSbS 1.60/400. Samples with a higher amount of S y lower percentage de Cu have a higher charge carrier concentration, since the compound is a *p*-type semiconductor, the holes are provided by the sulfur atoms.

The mobility of the samples is in accordance with the charge carrier concentration, at greater amount of this, the mobility decreases since there are interactions between the material lattice and the charge carriers themselves. A high charge carrier concentration leads to low electrical resistivity and high conductivity, like that reported for tetrahedrite.

The highest electrical conductivity was  $4.378 \times 10^2 \text{ (1/}\Omega\text{cm)}$  for the CuSbS 2.00/300 sample which contains a considerable percentage of chalcocite. However, the charge carrier concentration is similar for all the samples as wells the conductivities, which allows to be in range where the highest value of *ZT* for a semiconductor can be reached ( $10^{19}$  to  $10^{21} \text{ cm}^{-3}$ )<sup>2,29</sup>.

### 3.6. Morphology of the samples (SEM analysis)

The morphology of the samples with the best values of the PF (CuSbS 2.00/300 and CuSbS 1.78/300) and of the samples with the highest values of Seebeck coefficient (CuSbS 1.78/350 and CuSbS 1.45/350) was studied by scanning electron microscope (SEM). The images obtained are shown in the Figure 7 (a-d). The images shown a continues and compact surface for all the samples with non-uniformly distributed grains on this. This type of morphology has been reported in other similar Cu-Sb-S films obtained by PVD<sup>8</sup>, E-beam

evaporation<sup>17</sup> and chemical bath deposition<sup>30</sup>. The length of the diameters of some grains was measured used ImageJ software and they were labeled in Figure 7. The CuSbS 1.78/300 sample presents a grain size in the range of 20 to 144 nm, with formation of aggregates. The aggregates have sizes of 526 to 628 nm approximately. For the CuSbS 2.00/300 sample the surface morphology is more continue than the first sample. The grain size has dimensions of 28 to 86 nm approximately without aggregates. The sample CuSbS 1.45/350 has dimensions of the grain size of 33 to 115 nm and presents the formation of aggregates with sizes of 395 to

**Table 3.** Thermoelectric properties of CuSbS samples.

Sample/ Annealing temperature	Carrier concentration $n_h$ ( $\text{cm}^{-3}$ )	Mobility $\mu$ ( $\text{cm}^2/\text{Vs}$ )	Resistivity $\rho$ ( $\Omega\text{cm}$ )	Conductivity $\sigma$ ( $1/\Omega\text{cm}$ )	Seebeck coefficient at 60 °C ( $\sim 333$ K) S ( $\mu\text{V/K}$ ) Thin film: 56.69 at 340 K <sup>17</sup>	Power factor $S^2\sigma$ ( $\mu\text{W}/\text{cm}^2\text{K}^2$ ) Thin film: 2.30 at 495 K <sup>17</sup>
CuSbS 2.00/250	$2.143 \times 10^{22}$	$3.610 \times 10^{-2}$	$9.438 \times 10^{-3}$	$1.060 \times 10^2$	76.0	0.61
CuSbS 1.45/250	$3.777 \times 10^{20}$	$5.438 \times 10^{-1}$	$1.857 \times 10^{-2}$	$5.385 \times 10^1$	97.0	0.51
CuSbS 2.00/300	$1.849 \times 10^{21}$	1.513	$2.285 \times 10^{-3}$	$4.378 \times 10^2$	72.5	2.30
CuSbS 1.78/300	$4.390 \times 10^{22}$	$3.435 \times 10^{-2}$	$4.256 \times 10^{-3}$	$2.340 \times 10^2$	86.9	1.77
CuSbS 2.00/350	$2.755 \times 10^{22}$	$5.557 \times 10^{-2}$	$4.319 \times 10^{-3}$	$2.316 \times 10^2$	63.0	0.92
CuSbS 1.78/350	$3.522 \times 10^{20}$	$7.071 \times 10^{-1}$	$2.131 \times 10^{-2}$	$4.693 \times 10^1$	139.0	0.91
CuSbS 1.60/350	$1.974 \times 10^{22}$	$5.539 \times 10^{-2}$	$6.258 \times 10^{-3}$	$1.598 \times 10^2$	72.7	0.85
CuSbS 1.45/350	$3.536 \times 10^{20}$	$5.810 \times 10^{-1}$	$1.855 \times 10^{-2}$	$5.391 \times 10^1$	125.0	0.84
CuSbS 2.00/400	$2.029 \times 10^{22}$	$2.123 \times 10^{-2}$	$1.600 \times 10^{-3}$	$2.340 \times 10^2$	59.4	0.83
CuSbS 1.60/400	$3.056 \times 10^{22}$	$2.896 \times 10^{-2}$	$8.344 \times 10^{-3}$	$1.199 \times 10^2$	73.0	0.64
CuSbS 1.45/400	$1.397 \times 10^{20}$	2.918	$1.885 \times 10^{-2}$	$5.320 \times 10^1$	121.4	0.78

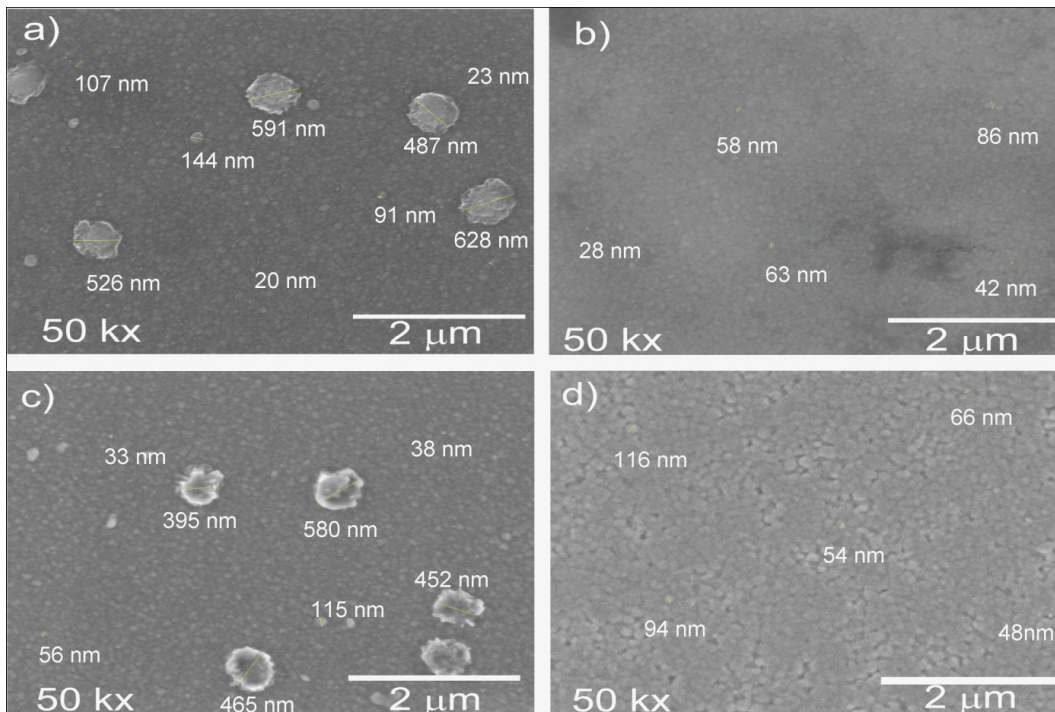


**Figure 7.** Surface images of CuSbS films; a) CuSbS 1.78/300, b) CuSbS 2.00/300, c) CuSbS 1.45/350 and d) CuSbS 1.78/350.

580 nm. Finally, the CuSbS 1.78/350 sample presents grain sizes of 48 to 116 nm without aggregates. The grain size is similar to that obtained by E-beam evaporation<sup>17</sup>; but lower than those obtained by evaporation and diffusion processes in layers<sup>8,15,31,32</sup>. This could be due to the thinner thicknesses of Sb<sub>2</sub>S<sub>3</sub> used in this investigation, which could favor the loss of material during annealing and therefore smaller grain sizes. In addition, the phase found in the highest proportion is tetrahedrite and, as can be seen in the works with which it is compared, they have a greater amount of chalcocite, and this has greater grain growth than the other phase mentioned.

The variation in the dimensions of the grain size indicates that the grain growth was not uniform throughout the film. But the grain sizes are similar for the four samples, which is consistent with XRD, with this analysis similar crystal sizes were obtained for all the samples. No significant effects of sulfide layer ratio or temperature are observed in the surface morphology of the films. In some cases, the effect of temperature on morphology has been described, where an increased in temperature favors the growth of larger grains; this due to coalescence<sup>8,33</sup>. In this case, it can be explained that the smaller grains combine with others and small empty spaces appears. This can be seen in Figure 7d, the small grains start to combine and empty spaces can be seen, in relation with Figure 7a, these samples have the same ratio of sulfides but different annealing temperature. Although the presence of tetrahedrite with smaller grains has also related to obtaining thin films by evaporation<sup>8,17</sup>; and all the samples present a high content of tetrahedrite.

Figure 8 shows the cross-sectional images of the a) CuSbS 2.00/300, b) CuSbS 1.45/350 and c) CuSbS 1.78/350 samples. The three samples only present growth in a single layer. There are no two layers that could be due to the precursors, this could indicate a complete diffusion between the sulfides used. The CuSbS 2.00/300 sample exhibits a compact morphology and a good adhesion with the substrate. The thickness film is of 440 nm approximately and is a value very close to that obtained by profilometry (420 nm). The difference may be due to equipment calibration (measurement uncertainty). For the CuSbS 1.45/350 sample, the morphology observed is compact in an only layer and with a good adhesion. The thickness of the film is of 430 nm approximately and is very close to the obtained by profilometry (450 nm). Finally, the CuSbS 1.78/350 sample presents a compact morphology in an only layer and a good adhesion to the substrate. The thickness

estimated is of 390 nm approximately and is close to that obtained by profilometry (410 nm).

### 3.7. XPS analysis

For the XPS analysis, all signals were adjusted to C1s which is associated with the adventitious hydrocarbon this peak es centered at 284.6 eV<sup>34</sup>. Additionally, Shirley's method was used to subtract the background of the signals. For the measurements, an Al K alpha source gun type was employed, an energy step size of 0.100 eV, a pass energy of 20.0 eV and a spot size of 650 μm. Figure 9a shows the high resolution (HR-XPS) signal for Cu 2p orbit. On the other side, one the most important aspects to the deconvolution method in the XPS analysis is the calculus of the difference in the binding energy ( $\Delta BE_{\text{element}}$ ). In that sense, the figure shows two signals at 951.56 and 932.06 eV that correspond at spin-orbit splitting of Cu 2p<sub>1/2</sub> and Cu 2p<sub>3/2</sub>, respectively. So, the  $\Delta BE_{\text{Cu}} = 19.5$  eV this value agrees to the value that was reported in a previous work<sup>8</sup>. The signals correspond to the Cu<sup>+</sup> valence state<sup>35</sup>. Figure 9b shows the XPS signals for Sb 3d species. The spectra show two signals with maximum intensity at 530.37 and 539.68 eV that correspond to the signals of Sb 3d<sub>5/2</sub> and Sb 3d<sub>3/2</sub><sup>8,36,37</sup> and is associated to the  $\Delta BE_{\text{Sb}} = 9.31$  eV close to the value that was reported by Medina-Montes et al.<sup>8</sup>. This first pair of peaks correspond to Sb<sup>5+</sup> and the other pair, with maximum intensity at 538.23 and 528.92 eV, correspond to Sb<sup>3+</sup>, with a  $\Delta BE_{\text{Sb}} = 9.31$  eV<sup>37</sup>. Finally, the Figure 9c shows the spectra for the S 2p species. In this case, two signals at 162.43 and 161.17 eV are observed, obtaining the  $\Delta BE_{\text{S}} = 1.26$  eV in agreement with previous work of our group<sup>38</sup>. These signals correspond at S 2p<sub>1/2</sub> and S 2p<sub>3/2</sub> respectively and correspond to S<sup>2-</sup><sup>37</sup>. According with the results, the valance of sates is very similar with another research, with Cu<sup>+</sup>, Sb<sup>3+</sup>, Sb<sup>5+</sup> and S<sup>2-</sup> in the formula  $Cu_{1.2}^+Sb_3^{3+}Sb_1^{5+}S_3^{2-}$ <sup>37</sup>; although our sample presents mixture of phases with chalcocite and sulfur deficiencies.

### 3.8. Seebeck coefficient and power factor

Table 3 shows the Seebeck coefficients and power factor (PF) of all samples. All samples have values of Seebeck coefficient greater than 50 μV/K and greater than those reported for thin films at 340 K<sup>17</sup>. The sample CuSbS 1.78/350 reached a maximum value of 139 μV/K, which agrees with the literature, at higher charge carrier concentration the value of *S* decrease<sup>2,29</sup>. The smallest value

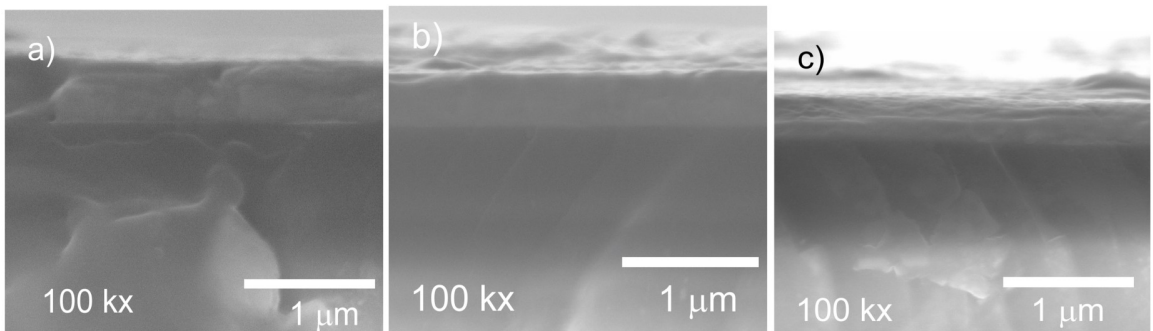


**Figure 8.** Transversal images of CuSbS films; a) CuSbS 2.00/300, b) CuSbS 1.45/350 and c) CuSbS 1.78/350.

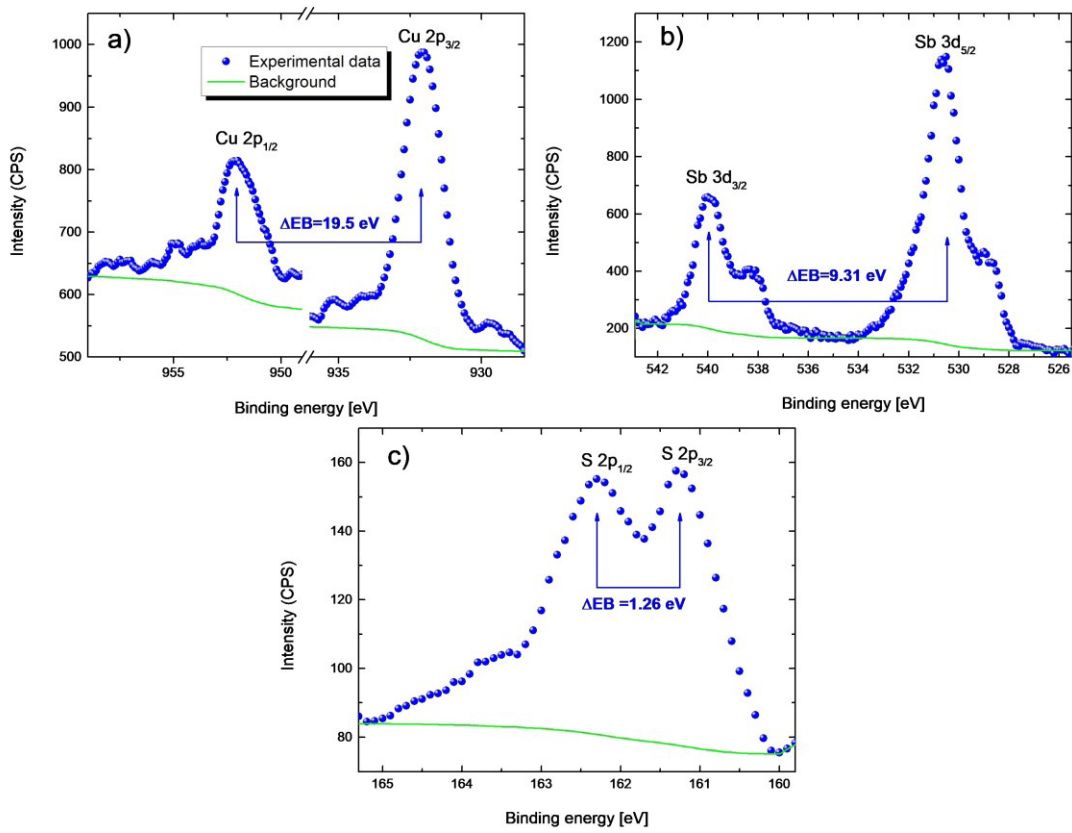


**Figure 9.** HR-XPS spectra of CuSbS 1.78/350 film; a) Cu 2p, b) Sb 3d and c) S 2p.

was for the CuSbS 2.00/400 sample that has a charge carrier concentration of  $2.029 \times 10^{22}$ .

Table 3 also presents the PF values for all samples. The greatest value was found in the CuSbS 2.00/300 sample ( $2.30 \mu\text{W}/\text{cm K}^2$ ) with a charge carrier concentration of  $1.849 \times 10^{21}$ . This is a similar value to that reported by another technique; however, the temperature differs, and a higher value could be reached. Also, in this work it was found that the sample contained mixtures of phases ( $\text{Cu}_{12}\text{Sb}_4\text{S}_{13}$  and  $\text{Cu}_3\text{Sb}_4\text{S}_4$ )<sup>17</sup>. On the other hand, the value of Seebeck coefficient is much lower in film than in bulk, where values of  $\sim 13.0 \mu\text{W}/\text{cm K}^2$  at 495 K have been reported. However, in this same work it is indicated that a direct comparison cannot be made and is necessary studies about the growth method and dynamics dependent stoichiometry<sup>17</sup>.

For the other samples, the value of PF decreases which coincides with the literature, a maximum value can be reached with a charge carrier concentration of  $10^{20} - 10^{21}$ <sup>29</sup>.

## 4. Conclusions

Thin films of  $\text{CuSbS}_2/\text{Cu}_{12}\text{Sb}_4\text{S}_{13}$  phases were obtained by a two-stage process, the sequential deposition of the  $\text{Sb}_2\text{S}_3$  and CuS layers on glass substrates, followed by annealing in a  $\text{N}_2$  atmosphere. It was found that the obtaining of the  $\text{CuSbS}_2$  or  $\text{Cu}_{12}\text{Sb}_4\text{S}_{13}$  phases depends on the thickness of the layers of the precursors and the annealing temperature. If the thickness of the CuS layer is increased and the  $\text{Sb}_2\text{S}_3$  layer is kept constant, the formation of  $\text{Cu}_{12}\text{Sb}_4\text{S}_{13}$  is favored by

increasing the annealing temperature. This due to a high Cu content in the samples, favored by the evaporation of S at high temperatures, which allows obtaining the tetrahedrite. However, the thermoelectric properties improved when both phases coexisted due to the combination of properties, such as the charge carries concentration and the electrical conductivity. The best value, in relation to the power factor, was  $2.30 \mu\text{W}/\text{cm K}^2$  at  $60^\circ\text{C}$  for a sample with a combination of  $\text{CuSbS}_2$  (34%) and  $\text{Cu}_{12}\text{Sb}_4\text{S}_{13}$  (66%). According to the results, it can be observed that a competitive thin film was obtained in comparison with others that have been obtained by other techniques. The techniques included spin coating and e-beam evaporation; with the advantage that the technique used in this work requires less time and does not require the manufacture of targets. The purity and stoichiometry of the  $\text{Cu}_{12}\text{Sb}_4\text{S}_{13}$  phase could be improved, using this method, by varying the thicknesses of  $\text{Sb}_2\text{S}_3$  and CuS layers; as well as modifying the annealing temperature and reducing anneal times to avoid sulfur loss. Also, the annealing process could be carried out in high pressure with an inert gas to avoid the loss of antimony and sulfur or in a closed system. Another option could be to carry out the annealing process in a sulfur atmosphere to enrich the samples with this element. However, according to the results, obtaining the pure phase does not guarantee an improve in the thermoelectric properties of the thin film compared to when both phases coexist. Finally, quantification of thermal conductivity is required to determine the ZT values of the samples.

## 5. Acknowledgments

The authors acknowledge the support from CONACYT and UAQ provided to the student Daniel Trejo Zamudio for his postgraduate studies. We acknowledge the technical support of Instituto de Energías Renovables, UNAM (José Campos R), for the Seebeck coefficient measurements and EDS analysis. To the FQST21 FQ-UAQ for financial support.

## 6. References

- Zhang X, Zhao L. Thermoelectric materials: energy conversion between heat and electricity. *J Mater*. 2015;1:92-105.
- Hamid Elsheikh M, Shnawah DA, Sabri MFM, Said SBM, Haji Hassan M, Ali Bashir MB, et al. A review on thermoelectric renewable energy: principle parameters that affect their performance. *Renew Sustain Energy Rev*. 2014;30:337-55.
- Sun F, Wu C-F, Li Z, Pan Y, Asfandiyar A, Dong J, et al. Powder metallurgically synthesized Cu<sub>12</sub>Sb<sub>4</sub>S<sub>13</sub> tetrahedrites: phase transition and high thermoelectricity. *RSC Advances*. 2017;7(31):18909-16.
- Keshavarz MK, Fattah-Alhosseini A. Effect of immersion time on corrosion behavior of single-phase alloy and nanocomposite bismuth telluride-based thermoelectrics in NaCl solution. *J Mater Eng Perform*. 2018;27(7):3386-93.
- Keshavarz MK, Fattah-alhosseini A. Electrochemical response of n-type bismuth telluride based thermoelectric materials in NaCl solutions: a comparison between a single-phase alloy and a nanocomposite containing MoS<sub>2</sub> nano-particles. *Arab J Chem*. 2020;13(1):1858-65.
- Fattah-alhosseini A, Keshavarz MK, Attarzadeh F. A study on the electrochemical responses of p-type bismuth telluride-based thermoelectric materials in a 0.1 M NaCl solution: comparing a nanocomposite with dispersed MoS<sub>2</sub> nanoparticles and a single-phase alloy. *J Alloys Compd*. 2020;815:152371.
- Baker J, Kumar RS, Sneed D, Connolly A, Zhang Y, Velisavljevic N, et al. Pressure induced structural transitions in CuSbS<sub>2</sub> and CuSbSe<sub>2</sub> thermoelectric compounds. *J Alloys Compd*. 2015;643:186-94.
- Medina-Montes MI, Campos-González E, Morales-Luna M, Sánchez TG, Becerril-Silva M, Mayén-Hernández SA, et al. Development of phase-pure CuSbS<sub>2</sub> thin films by annealing thermally evaporated CuS/Sb<sub>2</sub>S<sub>3</sub> stacking layer for solar cell applications. *Mater Sci Semicond Process*. 2018;80:74-84.
- Yang B, Wang L, Han J, Zhou Y, Song H, Chen S, et al. CuSbS<sub>2</sub> as a promising earth-abundant photovoltaic absorber material: a combined theoretical and experimental study. *Chem Mater*. 2014;26(10):3135-43.
- Riha SC, Koegel AA, Emery JD, Pellin MJ, Martinson ABF. Low-temperature atomic layer deposition of CuSbS<sub>2</sub> for thin-film photovoltaics. *ACS Appl Mater Interfaces*. 2017;9(5):4667-73.
- Welch AW, Zawadzki PP, Lany S, Wolden CA, Zakutayev A. Self-regulated growth and tunable properties of CuSbS<sub>2</sub> solar absorbers. *Sol Energy Mater Sol Cells*. 2015;132:499-506.
- Wan L, Ma C, Hu K, Zhou R, Mao X, Pan S, et al. Two-stage co-evaporated CuSbS<sub>2</sub> thin films for solar cells. *J Alloys Compd*. 2016;680:182-90.
- Hussain A, Ahmed R, Ali N, Shaari A, Luo J-T, Fu YQ. Characterization of Cu<sub>3</sub>SbS<sub>3</sub> thin films grown by thermally diffusing Cu<sub>2</sub>S and Sb<sub>2</sub>S<sub>3</sub> layers. *Surf Coat Tech*. 2017;319:294-300.
- Tang C, Liang D, Li H, Luo K, Zhang B. Preparation and thermoelectric properties of Cu<sub>18</sub>S/CuSbS<sub>2</sub> composites. *J Adv Ceram*. 2019;8(2):209-17.
- Chalapathi U, Poornaprakash B, Ahn CH, Park S-H. Two-stage processed CuSbS<sub>2</sub> thin films for photovoltaics: Effect of Cu/Sb ratio. *Ceram Int*. 2018;44(12):14844-9.
- Trejo-Zamudio D, Mayen-Hernandez SA, Quinones-Galvan JG, Moure-Flores FJ, Gómez-Herrera ML, Santos-Cruz J. Optoelectrothermoelectric properties of ternary chalcogenides thin films of CuSbS<sub>2</sub> and Cu<sub>12</sub>Sb<sub>4</sub>S<sub>13</sub>. In: 18th International Conference on Electrical Engineering, Computing Science and Automatic Control (CCE). New York: IEEE; 2021. p. 1-5.
- Prem Kumar DS, Ren M, Osipowicz T, Mallik RC, Malar P. Tetrahedrite (Cu<sub>12</sub>Sb<sub>4</sub>S<sub>13</sub>) thin films for photovoltaic and thermoelectric applications. *Sol Energy*. 2018;174:422-30.
- Du B, Zhang R, Chen K, Mahajan A, Reece MJ. The impact of lone-pair electrons on the lattice thermal conductivity of the thermoelectric compound CuSbS<sub>2</sub>. *J Mater Chem A Mater Energy Sustain*. 2017;5(7):3249-59.
- Rath T, MacLachlan AJ, Brown MD, Haque SA. Structural, optical and charge generation properties of chalcostibite and tetrahedrite copper antimony sulfide thin films prepared from metal xanthates. *J Mater Chem A Mater Energy Sustain*. 2015;3(47):24155-62.
- Kharbish S, Libowitzky E, Beran A. Raman spectra of isolated and interconnected pyramidal XS<sub>3</sub> groups (X = Sb, Bi) in stibnite, bismuthinite, kermesite, stephanite and bournonite. *Eur J Mineral*. 2009;21(2):325-33.
- Hurma T, Kose S. XRD Raman analysis and optical properties of CuS nanostructured film. *Optik (Stuttg)*. 2016;127(15):6000-6.
- Dinnebier RE, Billinge SJL. Powder diffraction, theory and practice. Cambridge: RSC Publishing; 2008.
- Wang W, Hao L, Zhang W, Lin Q, Zhang X, Tang Z. Preparation of CuSbS<sub>2</sub> thin films by a facile and low-cost chemical solution method. *J Mater Sci Mater Electron*. 2018;29(5):4075-9.
- Ornelas-Acosta RE, Avellaneda D, Shaji S, Castillo GA, Das Roy TK, Krishnan B. CuSbS<sub>2</sub> thin films by heating Sb<sub>2</sub>S<sub>3</sub>/Cu layers for PV applications. *J Mater Sci Mater Electron*. 2014;25(10):4356-62.
- Heavens OS. Optical properties of thin solid films. New York: Dover Publications; 1991.
- van Embden J, Latham K, Duffy NW, Tachibana Y. Near-infrared absorbing Cu<sub>12</sub>Sb<sub>4</sub>S<sub>13</sub> and Cu<sub>3</sub>SbS<sub>4</sub> nanocrystals: synthesis, characterization, and photoelectrochemistry. *J Am Chem Soc*. 2013;135(31):11562-71.
- Tablero C. Electronic and optical property analysis of the cu-sb-s tetrahedrites for high-efficiency absorption devices. *J Phys Chem C*. 2014;118(28):15122-7.
- Borup KA, de Boor J, Wang H, Drymiotis F, Gascoin F, Shi X, et al. Measuring thermoelectric transport properties of materials. *Energy Environ Sci*. 2015;8(2):423-35.
- Snyder GJ, Toberer ES. Complex thermoelectric materials. *Nat Mater*. 2008;7(2):105-14.
- Loranca-Ramos FE, Diliégros-Godines CJ, Silva González R, Pal M. Structural, optical and electrical properties of copper antimony sulfide thin films grown by a citrate-assisted single chemical bath deposition. *Appl Surf Sci*. 2018;427:1099-106.
- Garza C, Shaji S, Arato A, Perez Tijerina E, Alan Castillo G, Das Roy TK, et al. p-Type CuSbS<sub>2</sub> thin films by thermal diffusion of copper into Sb<sub>2</sub>S<sub>3</sub>. *Sol Energy Mater Sol Cells*. 2011;95(8):2001-5.
- Vinayakumar V, Shaji S, Avellaneda D, Aguilar-Martínez JA, Krishnan B. Copper antimony sulfide thin films for visible to near infrared photodetector applications. *RSC Advances*. 2018;8(54):31055-65.
- Ahmadipour M, Ain MF, Ahmad ZA. Effects of annealing temperature on the structural, morphology, optical properties and resistivity of sputtered CCTO thin film. *J Mater Sci Mater Electron*. 2017;28(17):12458-66.
- Morales-Luna M, Arvizu MA, Pérez-González M, Tomás SA. Effect of a CdSe layer on the thermo- and photochromic properties of MoO<sub>3</sub> thin films deposited by physical vapor deposition. *J Phys Chem C*. 2019;123(28):17083-91.

35. Amri A, Duan X, Yin C-Y, Jiang Z-T, Rahman MM, Pryor T. Solar absorptance of copper–cobalt oxide thin film coatings with nano-size, grain-like morphology: optimization and synchrotron radiation XPS studies. *Appl Surf Sci.* 2013;275:127-35.
36. Vinayakumar V, Shaji S, Avellaneda D, Das Roy TK, Castillo GA, Martinez JAA, et al.  $\text{CuSbS}_2$  thin films by rapid thermal processing of  $\text{Sb}_2\text{S}_3$ -Cu stack layers for photovoltaic application. *Sol Energy Mater Sol Cells.* 2017;164:19-27.
37. Wang L, Yang B, Xia Z, Leng M, Zhou Y, Xue D, et al. Synthesis and characterization of hydrazine solution processed  $\text{Cu}_{12}\text{Sb}_4\text{S}_{13}$  film. *Sol Energy Mater Sol Cells.* 2016;144:33-9.
38. Medina-Montes MI, Baldenegro-Pérez LA, Morales-Luna M, Sánchez TG, Santos-Cruz D, Mayén-Hernández SA, et al. Physical properties of photoconductive Ag-Sb-S thin films prepared by thermal evaporation. *Mater Sci Semicond Process.* 2022;137:106167.